Energy & Environmental Science

PAPER

View Article Online
View Journal | View Issue

Cite this: *Energy Environ. Sci.*, 2014, **7**, 3666

Organic photoelectrochemical cells with quantitative photocarrier conversion†

Antonio Guerrero,[a] Marta Haro,[a] Sebastiano Bellani,[b] Maria Rosa Antognazza,[b] Laura Meda,[c] Sixto Gimenez*[a] and Juan Bisquert*[ad]

Received 10th June 2014
Accepted 7th August 2014

DOI: 10.1039/c4ee01775g

www.rsc.org/ees

Efficient solar-to-fuel conversion could be a cost-effective way to power the planet using sunlight. Herein, we demonstrate that Organic Photoelectrochemical Cells (OPECs) constitute a versatile platform for the efficient production of solar fuels. We show that the photogenerated carriers at the organic active layer can be quantitatively extracted to drive photoelectrochemical reactions at the interface with a liquid solution. Indeed, an unprecedented photocurrent of 4 mA cm^{-2} is extracted for an OPEC device, comparable to that of a solid-state device with similar optical properties. Through the careful choice of the selective contact and the redox couple in the liquid medium, we can tune the energetics of the system and activate either oxidative or reductive chemistry. The design rules to drive the desired electrochemical reaction are provided based on a comprehensive study of the energetic aspects of OPEC configuration. Finally, we demonstrate that OPEC devices effectively produce hydrogen in acetonitrile when a cobaloxime based homogeneous catalyst is present in the solution, and HCl is used a source of protons.

Introduction

Converting the energy of solar photons into chemical bonds is termed solar fuel production. This is the purpose of photoelectrochemical cells (PECs) that aim to convert abundant compounds dissolved in liquid medium into useful fuels through electrochemical reactions powered only by solar photons.[1] Reduction of CO_2 by similar means is also of great interest for environmental purposes. The realization of a cost-effective device would be a major step towards reliable renewable energy economy, however this has not yet been achieved. Recently, the quest for semiconductors that fulfil the light absorption, charge separation properties and adequate energy levels for realizing the required photoelectrochemical reactions in combination with suitable surface catalysts, has driven a great research effort. However, so far the main stream of research in materials and processes involves either metal oxide inorganic semiconductors such as TiO_2,[2] Fe_2O_3,[3] WO_3 [4] and $BiVO_4$ [5] or conventional photovoltaic materials such as Si and $CuIn_{1-x}Ga_xSe_2$ (CIGS).[6]

Meanwhile, organic photovoltaic materials have experienced extraordinary development with great potential to produce inexpensive devices. The organic bulk heterojunction (BHJ) operation is based on ultrafast transference of carriers from an absorbing polymer or small organic molecule to a functionalized fullerene.[7] Intermediate efficiency BHJ cells, such as the archetypal combination poly(3-hexylthiophene):[6,6]-phenyl C_{61}-butyric acid methyl ester (P3HT:PCBM) can provide up to $\approx$10 mA cm^{-2} photocurrent, 0.63 V open circuit voltage, and high fill factor using a standard configuration. Careful combination of improvements in the latest generation devices, such as optimization of donor–acceptor blend morphology, synthesis of low bandgap molecules that show increased light absorption, and improvement of transport properties and selective contacts, has provided large solar to electricity conversion efficiencies of around 10%.[8,9] The progress of organic cells demonstrates the versatility of organic photovoltaic materials, which can be designed and improved to realize highly efficient devices.

Despite these developments, the application of photoactive organic materials for solar fuel production has been marginally explored. The use of BHJ blend materials in solar fuel production requires that two fundamental conditions are satisfied: (i) the organic blend must preserve the capability of generating charges even when it is in direct contact with a liquid electrolyte; (ii) the photovoltage must be high enough to allow efficient charge transfer between the organic film and the electrolyte.

[a]*Photovoltaics and Optoelectronic Devices Group, Departament de Fisica, Universitat Jaume I, 12071 Castello, Spain. E-mail: sjulia@uji.es; bisquert@uji.es*

[b]*Center for Nano Science and Technology @Polimi, Istituto Italiano di Tecnologia, Via Pascoli 70/3, 20133 Milano, Italy*

[c]*ENI-Donegani Institute, Research Center for Non-Conventional Energies, Via Fauser 4, 28100 Novara, Italy*

[d]*Department of Chemistry, Faculty of Science, King Abdulaziz University, Jeddah, Saudi Arabia*

† Electronic supplementary information (ESI) available: Shuttered *J–V* curves of additional IFL/BHJ/redox couple configurations, magnification of the area of inversion of the photocurrent in Fig. 3, stability tests and labeling experiments. See DOI: 10.1039/c4ee01775g

The coupling of photogeneration in organic conductors and blends with liquid electrolytes has been investigated for a long time,[10–15] but the obtained photocurrents have been significantly lower compared to those expected from the light harvesting efficiency, evaluated through optical absorbance measurements. Additionally, the mechanisms leading to gas evolution remain controversial. Consequently, a detailed understanding of the interfacial processes is urgently needed, in order to fill the gap between the theoretically achievable photocurrent (on the base of conventional organic solar cells) and practical results obtained with photoelectrochemical cells.[10,16–18]

PEC conversion requires the combination of three factors. First is that the photovoltaic material in contact with a liquid medium must function efficiently in terms of light absorption, internal charge separation, and transport to the active surface. Second, the band edge positions should be appropriately located to allow electron (hole) transfer to the solution to be reduced (oxidised). The third requirement is that the interfacial charge transfer must occur at a significant pace when the surface is in contact with the relevant compound to be transformed into a fuel, *e.g.*, water or CO_2. This last issue may require the assistance of a catalyst that facilitates the given electrochemical reaction. Unfortunately, to date these factors have not been comprehensively studied in an Organic Photoelectrochemical Cell (OPEC) configuration.

In summary, it is first necessary to demonstrate that the BHJ photovoltaic blend operates efficiently when the liquid medium replaces one of the metal contacts of the solar cell. In this paper we address this question and we show a high current and voltage of standard P3HT:PCBM blends in contact with different electrolytes. We investigate the internal processes of photon-to-carrier conversion at the organic/liquid interface and we show inversion of photocurrent depending on the nature of the contacts and redox couple. Furthermore, we demonstrate photocurrents of hydrogen generation of 1 mA cm^{-2} when cobaloxime based catalysts are introduced in the solution. This study demonstrates the high potential of OPECs for solar fuel production.

Results and discussion

The first step in our study is to understand if there is a fundamental limitation in the photogeneration and charge extraction of carriers when a liquid electrolyte is in contact with the organic active layer. With this objective in mind, we prepared devices mimicking those known to work efficiently as BHJ solar cells (Fig. 1a). In this configuration ZnO and MoO_3 act as interfacial layers (IFL) selective to electrons and holes, respectively. Fig. 1c shows the current density–voltage characteristics of representative organic BHJ solar cells with the structure ITO/ZnO/P3HT:PCBM/MoO_3/Ag. These cells show the standard electrical characteristics for this type of device widely reported in the literature.[19] When a thick layer of silver (100 nm) is used, the back contact acts as a mirror, reflecting some of the incident light, increasing the effective incident path length. On the other hand, when a thin layer of silver (20 nm) is used, the device is

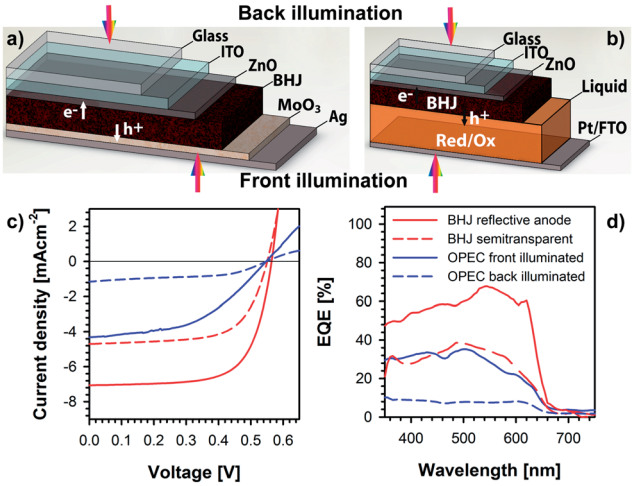

Fig. 1 (a) Device architecture of a BHJ solar cell and (b) Organic Photoelectrochemical Cell (OPEC). The illumination direction for both devices is indicated. The main difference in the OPEC configuration is the presence of a liquid solution with a redox couple able to extract carriers to the solution. (c) Current density–voltage characteristics and (d) External Quantum Efficiency (EQE) of devices fabricated in both configurations. Reflective and semi-transparent BHJ refers to devices with 100 nm and 20 nm thick Ag layer, respectively.

semitransparent and the light harvesting at the active layer is decreased, explaining the lower photocurrent observed.

In the OPEC configuration the absorber layer is in contact with a liquid electrolyte and the result of the photocurrent is to drive an interfacial reaction at the solid–liquid contact. Ultimately such reaction must provide a useful fuel, however in the present study we first focus the study on facile electrochemical reactions that show the operation of the photoactive organic blend in contact with a liquid medium.

Thus the hole selective layer, MoO_3, was replaced by a redox couple able to accept holes from the active organic electrode in an organic solvent with a large electrochemical window (Fig. 1b). In particular, an acetonitrile solution is used containing ferrocene–ferrocene$^+$ (Fc–Fc$^+$) as the redox couple and tetrabutyl ammonium hexafluorophosphate ($N(Bu^n)_4PF_6$) as the support electrolyte. When the MoO_3/Ag contact is replaced by the Fc–Fc$^+$ redox couple in the OPEC configuration with a Pt counter-electrode, a sizeable photocurrent of 4 mA cm^{-2} is observed, which is to the best of the authors' knowledge, the highest current reported in an all-organic PEC device. Interestingly, both semitransparent BHJs and OPECs show similar photoconversion properties as reflected by the external quantum efficiencies (EQE) in Fig. 1d. In addition, when the OPEC device is illuminated through the electrolyte, the photocurrent drops to about 1 mA cm^{-2} due to the optical losses at the cell chamber. All these results clearly indicate that the OPEC device realizes quantitative carrier extraction to the electrolyte comparable to that of an optimized metal contact. An improvement of the optical engineering of the device may lead to enhanced photocurrents.

The rational design of an OPEC able to transform the incoming solar energy into chemical energy entails the

adequate selection of the interfacial layer (IFL) and redox couple: this would allow efficient extraction of electrons or holes to the electrolyte solution through a specific chemical reaction. For this purpose, two interfaces should be considered, both the IFL/organic blend and the organic blend/electrolyte interfaces. The first one has been intensively studied in organic photovoltaic devices since the energy level equilibration at the contacts determines the confinement of the electrical field providing efficient collection of carriers.[20–23] Furthermore, considering other kinds of photoelectrochemical cells (based on colloidal quantum dots), it has been recently demonstrated that the selection of an adequate IFL can determine the sign of the photovoltage, *i.e.* the direction of the photogenerated charges (electrons and holes) that are driven to the collector and to the solution.[24] With these results in mind, we have selected a hole (ZnO) and an electron (PEDOT:PSS) blocking layer as the IFL in our OPEC devices. For the selection of the redox couples, Marcus theory[25,26] has been considered and the Fc–Fc^+ redox potential (4.9 eV) matches well with the HOMO level of the polymer (5.0 eV) and benzoquinone–benzoquinone^{-} (BZQ–BZQ^{-}) (with a redox potential 4.0 eV close to the LUMO of the fullerene, 3.2 eV). Consequently, both systems, Fc–Fc^+ and BZQ–BZQ^{-} have been selected as hole and electron acceptors, respectively.

In order to elucidate whether the organic active layer is able to photogenerate a similar charge density in both PV and OPEC configurations, continuous-wave photoinduced absorption (CW-PIA) spectroscopy experiments were carried out. CW-PIA monitors the change in the transmission spectrum of the organic active layer due to the absorption of long-lived (>10 μs) charged states. Hence, P3HT provides a spectroscopic fingerprint, which allows the quantification of the occurrence of polarons in the presence of a redox electrolyte in contact with the organic blend. Polarons are localized defects generated by an introduced charge carrier – electron or hole – into a polymer together with the consequent polarization locally centered on the charge.[27] These polarons have associated energy quantum states, which are responsible for the CW-PIA spectra. Fig. 2 shows representative "in-phase" and "out-of-phase" CW-PIA spectra of the ITO/ZnO/BHJ and ITO/PEDOT:PSS/BHJ systems in air and in contact with a liquid medium. The excited state photophysics of the P3HT/PCBM blend has been extensively studied in air, allowing the identification of the broad absorption between 620–1100 nm as the overlapping of two polaron absorption bands, with peaks at 780 nm (free polarons) and 960 nm (localized polarons).[28] Fig. 2a shows that, when the electrode ITO/ZnO/BHJ is immersed in an electrolyte solution containing the Fc–Fc^+ redox couple, the polaronic fingerprint of P3HT matches the signal obtained in air, suggesting that charge generation within the organic BHJ is not altered by the presence of the liquid electrolyte. Similar results have been previously obtained in PPV-based polymers in contact with aqueous electrolytes, focusing however on much shorter timescales, relevant for charge generation processes.[29] On the other hand, when the ITO/PEDOT:PSS/BHJ system is immersed in the BZQ–BZQ^{-} solution (Fig. 2b), the broad signal in the in-phase spectrum increases compared to that obtained in air and a clear response is observed in the out-of-phase spectrum (assigned to the absorption of very long-lived species). These two differences suggest longer photogenerated carrier lifetimes and can be ascribed to the presence of surface states.[30,31] However, other causes that can increase the lifetime of the photogenerated charges cannot be excluded, namely, photoactivated doping that leads to more hydrophilic surfaces that change the electrostatic interactions, or else screening of the electric field probably due to a different orientation of the chains.[32]

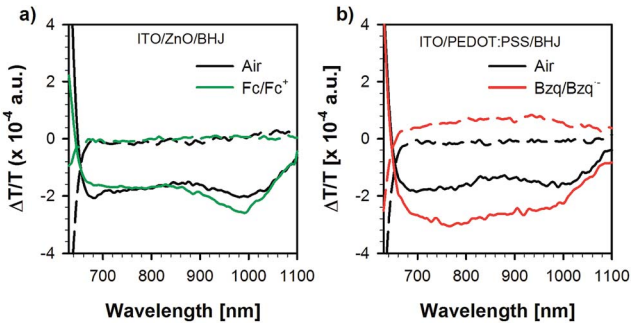

Fig. 2 Continuous-wave photo-induced absorption spectra of (a) ITO/ZnO/BHJ and (b) ITO/PEDOT:PSS/BHJ in air and in the presence of Fc–Fc^+ and BZQ–BZQ^{-} redox couples, respectively. Solid lines correspond to in-phase response and dashed lines to out-of-phase response. The optical excitation at 561 nm and a modulation frequency of 133 Hz.

CW-PIA measurements of the systems immersed in the electrolyte solutions were repeated after 20 minutes, with identical results, indicating that no degradation phenomena affecting the photogeneration of charges in the organic blend take place within this time scale. This result is in good agreement with the stability test described below. All in all, these results suggest that the presence of a liquid electrolyte containing a redox couple does not significantly affect the photogeneration process in the active layer BHJ, increasing the polaron lifetime when BZQ–BZQ^{-} acts as an electron scavenger.

The energetic aspects of the OPEC system have been studied using a three-electrode configuration, with a Ag/Ag^+ reference electrode, a graphite rod as the counter-electrode and the system under study as the working electrode. Fig. 3 shows the *J*–*V* plots under chopped illumination for the designed systems to inject holes and electrons into the solution, ITO/ZnO/BHJ/Fc–Fc^+ and ITO/PEDOT:PSS/BHJ/BZQ–BZQ^{-}, respectively (additional ITO/IFL/redox couple combinations are shown and discussed in the ESI, Fig. S1†). Fig. 3a shows that the hole photocurrent (positive photocurrent) increases at positive bias indicating holes injected into the solution upon illumination and nearly 4 mA cm^{-2} is achieved at +1 V *vs.* Fc–Fc^+. Moreover, the dark current is low indicating that the electrolyte and redox couple efficiently block the injection of electrons into the solution, as expected for a selective contact. Interestingly, at voltages close to −1 V *vs.* Fc–Fc^+ we observe an inversion of the photocurrent, indicating that electrons are collected by the solution. We show a magnified area of the region where inversion of the photocurrent takes place in the ESI, S2.† This inflexion point is related to the flatband potential V_{fb}, which is

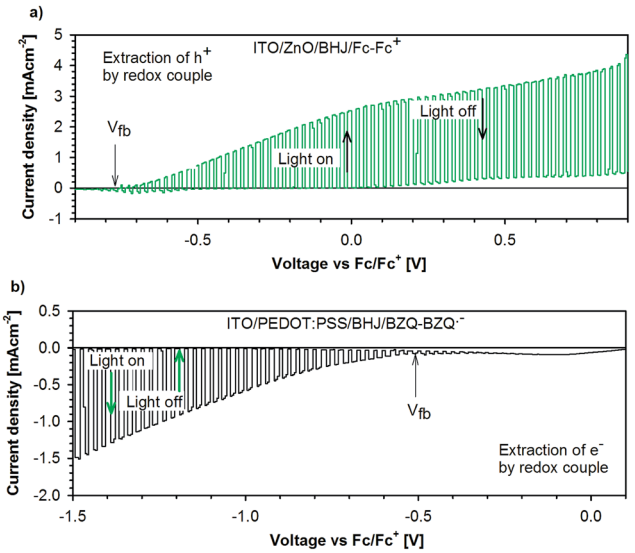

Fig. 3 Shuttered J–V curves in acetonitrile (0.1 M tetrabutyl hexafluorophosphate) recorded at 5 mV s^{-1} for ITO/PEDOT:PSS/BHJ/Fc–Fc^+ (a) and ITO/ZnO/BHJ/BZQ–$BZQ^{\cdot-}$ (b). The flatband potential (V_{fb}) extracted from Mott–Schottky analysis (see Fig. 4) is also indicated. A magnified view of the region where inversion of the photocurrent takes place is presented in the ESI, S2.†

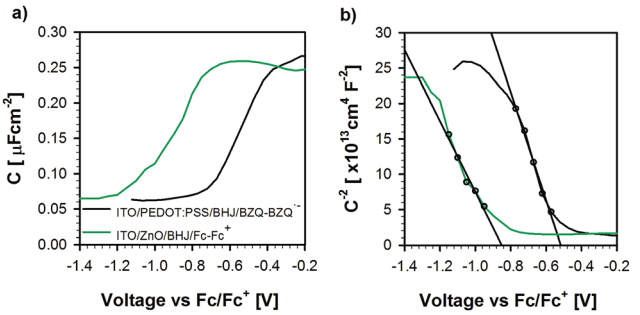

Fig. 4 Capacitance–voltage response (a) and Mott–Schottky analysis (b) of ITO/PEDOT:PSS/BHJ in the presence of BZQ–$BZQ^{\cdot-}$ redox couple and ITO/ZnO/BHJ in contact with the Fc–Fc^+ redox couple.

the applied potential required to remove pre-existing band-bending at the semiconductor interface. Indeed, this effect of inversion of the photocurrent has been previously observed in lightly doped systems.[33] Similarly, Fig. 3b shows the increase in the electronic photocurrent (negative photocurrent) in the cathodic sweep indicating the injection of electrons from the system ITO/PEDOT:PSS/BHJ to the BZQ–$BZQ^{\cdot-}$ redox couple with practically zero dark current and a turn-on voltage of the photocurrent related to the position of V_{fb}. Again, the obtained photocurrent density is in the order of mA cm^{-2}. These results demonstrate that the desired charge carriers can be injected into the electrolyte solution with an adequate selection of both IFL and redox couple. Importantly, OPEC devices based on the configuration ITO/ZnO/BHJ/Fc–Fc^+ constitute robust and stable devices as evidenced by the chronoamperometry curve obtained during a period of 6 h under shuttered illumination, presented in the ESI (Fig. S3†). Devices based on the configuration ITO/PEDOT:PSS/BHJ/BZQ–$BZQ^{\cdot-}$ were somehow less stable, we are currently investigating the reasons for this degradation.

In order to further understand the carrier dynamics of the devices, we performed capacitance–voltage measurements in the three-electrode configuration. In these experiments, the working electrode is driven at a DC voltage and a small AC perturbation (1 kHz) is applied, the differential current output is measured and the capacitance is extracted. A single frequency is selected, since the capacitance was observed to be frequency independent in the range of 100 Hz to 10 kHz. Representative capacitance–voltage measurements under dark conditions for two OPEC configurations are shown in Fig. 4. These results are similar to those typically observed in OPVs: a constant capacitance that increases at intermediate applied voltages and equilibrates towards positive values. This behaviour is generally observed for p-doped systems and has been previously correlated with the presence of a depleted layer at the organic layer/cathode interface.[34] From the Mott–Schottky analysis (C^{-2} *versus* V) the doping density (n) of the active layer can be extracted. The results for a selection of device configurations are shown in Table 1. Values of n are similar to those previously observed in regular OPVs ($n = 1$–10×10^{16} cm^{-3}) indicating that the presence of the liquid solution does not substantially modify the presence of electrically active impurities in the BHJ layer. Note that a different behaviour was observed in contact with aqueous saline electrolytes.[35] Although the doping density is related to the properties of the polymer itself, the obtained values are moderately increased by the use of a nano-sized porous ZnO layer that seems to restrict the domain size of the P3HT increasing the values of n.[36] In addition, doping values are uncorrelated with the redox couple used during the measurement.

On the other hand, the intercepts of the straight line with the x-axis define the values of V_{fb} collected in Table 1. At this applied voltage, bands will be flat and collection of carriers at the contacts will not be favoured as carriers will only reach the contacts by diffusion. This explains the very low photocurrent values close to V_{fb} in Fig. 3. We note that the values of V_{fb} are strongly dependent on the work function of the interfacial layer and the redox potential of the electrolyte solution is in good agreement with previous studies.[22]

Fig. 5 depicts the basic elements of the energetic landscape of both the optimized OPEC devices (ZnO/BHJ/Fc–Fc^+ and PEDOT:PSS/BHJ/BZQ–$BZQ^{\cdot-}$), showing first the energy levels of the separate materials at a constant vacuum level, and then

Table 1 Summary of doping density (n) and flat band potential (V_{fb}) extracted from capacitance–voltage data for selected OPEC configurations

IFL	Redox couple	n [$\times 10^{16}$ cm^{-3}]	V_{fb} [V *vs.* Fc–Fc^+]
ZnO	Fc–Fc^+	14.1	−0.851
PEDOT:PSS	Fc–Fc^+	5.4	−0.490
PEDOT:PSS	BZQ–$BZQ^{\cdot-}$	6.17	−0.516
ZnO	BZQ–$BZQ^{\cdot-}$	38.0	−0.871

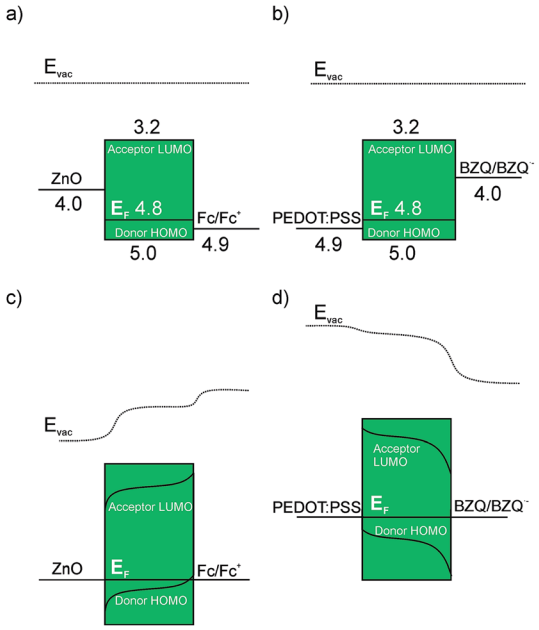

Fig. 5 Energy level diagrams representing both high performing OPEC configurations before and after electrical equilibration. The vacuum level is also included. All numbers are referred to eV with respect to the vacuum level (a) ZnO/BHJ/Fc–Fc^+ before electrical equilibration, (b) PEDOT:PSS/BHJ/BZQ–BZQ^- before electrical equilibration, (c) ZnO/BHJ/Fc–Fc^+ after electrical equilibration, and (d) PEDOT:PSS/BHJ/BZQ–BZQ^- after electrical equilibration. In (a) and (c) ZnO acts a selective contact for electrons and Fc–Fc^+ produces a band bending at the BHJ/solution interface enabling the extraction of holes to the solution. In (b) and (d) PEDOT:PSS acts as selective contact for holes and BZQ–BZQ^- induces band bending to extract electrons from the organic layer to the solution.

showing the equilibrated junctions at flat Fermi level. The values for the work function of the Fc–Fc^+ and BZQ–BZQ^- redox couples have been obtained by cyclic voltammetry and those for the organic blend, ZnO and PEDOT:PSS have been extracted from literature.[22,37,38] In these diagrams, we have considered a slightly doped organic semiconductor material ($n \sim 10^{16}$ cm^{-3}), no surface states and a concentration of the redox couple high enough (>0.1 M) to assume that the potential drop fully takes place within the semiconductor material at the BHJ/solution interface.[39] Fig. 5c and (d) illustrate the modification of the energy levels after contact equilibration of the system ITO/ZnO/BHJ/Fc–Fc^+ and PEDOT:PSS/BHJ/BZQ–BZQ^-, respectively. The working mechanism of BHJ solar cells with ZnO and PEDOT:PSS interfacial layers is well-established.[40,41] In those systems the energy levels are well located to drive the photogenerated electrons to the ZnO contact and holes to the PEDOT:PSS. In the OPEC configuration the role of Fc–Fc^+ is similar to that of PEDOT:PSS, since they both exhibit a similar redox potential and work function. We believe that in these conditions the semiconductor is working under accumulation (the Fermi level intercepts the maximum of the valence band). On the other hand, the system ITO/PEDOT:PSS/BHJ/BZQ–BZQ^- can drive the photogenerated electrons to the electrolyte solution and the holes to the IFL. These schemes are in good agreement with the photoelectrochemical behavior presented in Fig. 3.

In order to complete our study, we demonstrate solar to fuel energy conversion with an OPEC device. For this purpose, the charge generated in the BHJ electrode is transferred to an homogeneous catalyst (chloro(pyridine)bis(dimethylclyoximate)cobalt III), which is soluble in acetonitrile and replaces the redox couple (benzoquinone). HCl is used as the proton source.

Cobaloximes are cobalt complexes showing powerful nucleophilic behaviour in their reduced state, Co(I). These complexes can be protonated to yield Co(III)-hydride species, which turn into H_2 molecules by either protonation of the hydride moiety or bimolecular reductive elimination.[42] This behaviour has been exploited to catalyze the hydrogen evolution reaction by electrochemical[43,44] or more recently photochemical systems.[45] Herein, we use for first time these complexes as intermediate catalysts to generate H_2 with the flux of photocarriers provided by an OPEC device.

The photoelectrochemical behaviour of ITO/PEDOT:PSS/BHJ in the presence of the cobaloxime (33 mM) and a proton donor (HCl, 5 mM) was first evaluated, Fig. 6. The modest HCl concentration guarantees that cobaloxime complexes are catalytically active.[43] In the dark, no current is measured due to the outstanding rectifying properties of the PEDOT:PSS IFL for electrons. Under illumination, the photocurrent follows the typical catalytic wave of cobaxolime complexes in the presence of a strong acid; *i.e.*: the photocurrent increases with the applied voltage and shows an irreversible peak due to electroreduction of protons, close to the Co(II)/Co(I) reversible wave.[43,46] The photocurrent peaks at −0.97 V *vs.* the Fc^+–Fc reference, which corresponds to 3.9 eV with respect to the vacuum level. This value is very close to the redox level of BZQ–BZQ^- (4.0 eV). Consequently, the energetics of the ITO/PEDOT:PSS/BHJ/cobaloxime system is adequate for efficiently driving the photogenerated electrons to the electrolyte solution. Furthermore, the photocurrent maximum (1.15 mA cm^{-2}), is similar to the value obtained when the BZQ–BZQ^- redox couple is used (Fig. 3b), as expected in the absence of kinetic barriers. Finally the production of H_2 in the ITO/PEDOT:PSS/BHJ/cobaloxime system was confirmed by labelling experiments. Details of these measurements can be found in the ESI, S4.† These results highlight the extraordinary potential of organic semiconductors for the

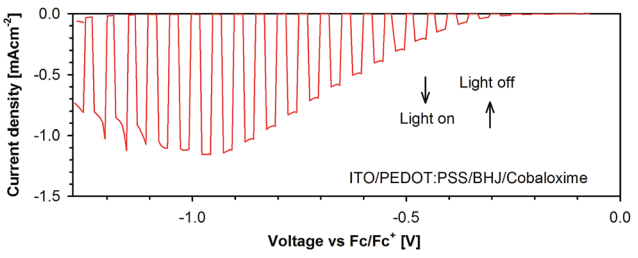

Fig. 6 Shuttered *J*–*V* curves in acetonitrile (0.1 M tetrabutyl hexafluorophosphate) recorded at 5 mV s^{-1} for ITO/PEDOT:PSS/BHJ/cobaloxime and 5 mM in HCl as proton source.

production of solar fuels and validate the developed design rules to provide OPEC systems with tailored electrochemical properties. The ultimate goal is exploiting this configuration in aqueous environments to carry out solar H_2 generation from water splitting and we are intensively working in this direction in our lab.

Conclusions

We have demonstrated that organic photoelectrochemical cells (OPECs) are able to quantitatively extract the photocurrent generated in the organic active layer. A record photocurrent of 4 mA cm^{-2} has been obtained for this device, which is to the best of the authors' knowledge the highest photocurrent obtained for an organic photoelectrochemical cell. We have showed that the photogenerated charge at the organic active layer is not affected by the presence of the liquid medium. Moreover, by a careful selection of the redox couple and the interfacial layer, the energetics of the system can be tailored so that the organic blend can provide a flux of either electrons or holes to the solution. Consequently, oxidative or reductive chemistry at the semiconductor/liquid interface can be activated upon demand expanding applicability of the system for the production of different solar fuels. These results can be satisfactorily explained on the basis of energy diagrams, which have been constructed with experimental data and Fermi level alignment. Finally, we demonstrate effective solar to H_2 conversion with an OPEC device coupled to an homogeneous cobaloxime based catalyst. The versatility of organic materials is a solid guarantee for further optimization of OPEC devices, which constitute a real low-cost alternative for the generation of solar fuels.

Methods

Materials

The following materials were used to prepare the OPV and OPEC electrodes: P3HT (Luminescence Technology Corp., MW > 45 000 (GPC)), $PC_{60}BM$ (Solenne, 99.5%), PEDOT:PSS (CLEVIOS P AI 4083), ZnO (Gene's Ink), MoO_3 (Aldrich, 99.9%), silver (Aldrich, 99.99%), ITO (PTB7 labs, 10 Ω sq^{-1}), and *o*-dichlorobenzene (Aldrich, 99.9%). All materials were used as received without further purification. For OPV fabrication, all manipulations were carried out in a glovebox under a nitrogen atmosphere, unless otherwise stated. P3HT:PCBM blends were prepared from dry *o*-dichlorobenzene (1 : 1, 34 mg mL^{-1}) and were stirred at 70 °C for 16 h before sample preparation. For the preparation of the electrolytic solutions acetonitrile (AlfaAesar, 99.8+%), ferrocene (Aldrich, 98.0%), benzoquinone (Fluka, 99.5%), and tetrabutyl hexafluorophosphate (Fluka, 99.0%) were used as received without further purification.

Device fabrication

Organic solar cells (OPVs) were fabricated in the configuration ITO/ZnO/P3HT:$PC_{60}BM$/MoO_3/Ag, with 25 mm^2 of active area. Pre-patterned ITO substrates were cleaned and UV-ozone treated. A ZnO nanoparticle solution was spin coated in air at 1000 rpm for 30 seconds followed by thermal treatment at 100 °C for 2 minutes to provide a ZnO layer thickness of ~40 nm. Substrates were transferred to a glovebox equipped with a thermal evaporator and were annealed at 120 °C for 5 minutes. The P3HT:$PC_{60}BM$ layer was deposited at a speed of 1200 rpm for 30 seconds and was placed in a petri dish to allow slow drying of the film during a period of 2 h to enable an adequate morphology of the blend. At this point, samples were thermally annealed at 130 °C for 10 min. Evaporation was carried out at a base pressure of 3×10^{-6} mbar to provide different thicknesses of MoO_3/Ag either 7.5/100 nm (reflective anode) or 7.5/20 nm (semitransparent anode). Devices were encapsulated with a photoresin and a glass microscopy slide. Samples were then taken out of the glovebox for device characterization. Similarly, OPEC electrodes in the configuration ITO/ZnO/P3HT:$PC_{60}BM$ were prepared as above using un-patterned ITO coated glass (4 cm^2) and avoiding the evaporation step. The counter electrode was prepared with chloroplatinic acid, H_2PtCl_6, in ethanol solution onto FTO glass and was heated in an oven at 450 °C for 30 min. A silicon spacer (50 μm thick) was used between the electrode and the counter electrode with a circular hollow space of area 0.26 cm^2 filled with the electrolyte solution. Alternatively, for electrodes replacing ZnO by PEDOT:PSS the spin coating step of PEDOT:PSS was carried out at 5500 rpm for 1 minute with a film thickness of ~35 nm.

Device characterization

Current density–voltage measurements of the photovoltaic devices showed in Fig. 1 were carried out by illumination with a 1.5G illumination source (100 mW cm^{-2}) using an Abet Sun 2000 Solar Simulator. The light intensity was adjusted with a calibrated Si solar cell. The photoelectrochemical characterization was performed in a three-electrode configuration, where a graphite bar and a Ag/Ag^+ ($AgNO_3$ 0.1 M in acetonitrile) were, respectively, used as the counter-electrode and reference. The distance between the working and counter-electrodes was 1 cm approximately. The electrolyte was a 0.1 M tetrabutylammonium hexafluorophosphate solution in acetonitrile with a redox pair ferrocene ($Fc–Fc^+$, 0.16 M) or benzoquinone ($BZQ–BZQ^-$, 0.2 M). The electrodes were illuminated through the substrate using a 300 W Xe lamp, where the light intensity was adjusted with a thermopile to 100 mW cm^{-2}. All potentials have been referred to the ferrocene redox potential: $E_{Fc–Fc^+} = E_{Ag/Ag^+} - 0.0716$. Capacitance–voltage measurements were performed with a PGSTAT-30 Autolab potentiostat equipped with a frequency analyzer module, and were recorded by applying a small voltage perturbation (20 mV rms). Measurements were carried out under dark conditions at a frequency of 1000 Hz. External Quantum Efficiency (EQE) measurements were performed at a short-circuit using a 150 W Xe lamp coupled with a monochromator controlled by a computer. The light intensity was measured using an optical power meter 70310 from Oriel Instruments where a Si photodiode was used to calibrate the system. Labelling experiments were carried out with a homemade sealed photoelectrochemical cell, where an Ar stream (~12 mL min^{-1}) was constantly flowing through the cell. The

electrode was immersed in the solution and illuminated through the electrolyte. The outlet gas was analyzed by an Agilent Technologies AG-490 gas chromatograph.

Continuous-wave photo-induced absorption spectra were performed in transmission geometry. A 560 nm laser diode served as the pump beam, modulated by a mechanical chopper at a frequency of 133 Hz. Transmission spectra are recorded using a probe beam from a Tungsten halogen lamp, focused on the sample by spherical mirrors in order to avoid chromatic aberrations. The transmitted light is dispersed with a monochromator and detected by a photodiode. The photoinduced variations of the transmission in the sample were recorded using a lock-in amplifier. All the differential spectra have been corrected for the photoluminescence and normalized by the transmission spectrum.

Competing financial interests

The authors declare no competing financial interests.

Acknowledgements

We acknowledge the financial support of the European Community through the Future and Emerging Technologies (FET) programme under the FP7, collaborative Project contract no. 309223 (PHOCS). MRA acknowledges contributions through the EU project OLIMPIA, FP7-PEOPLE-212-ITN 316832 and by national grant Telethon – Italy, Grant no. GGP12033. We would like to thank Gene's Ink for the supply of ZnO nanoparticles.

References

1 M. G. Walter, E. L. Warren, J. R. McKone, S. W. Boettcher, Q. Mi, E. A. Santori and N. S. Lewis, *Chem. Rev.*, 2010, **110**, 6446–6473.
2 M. Ni, M. K. H. Leung, D. Y. C. Leung and K. Sumathy, *Renewable Sustainable Energy Rev.*, 2007, **11**, 401–425.
3 T. W. Hamann, *Dalton Trans.*, 2012, **41**, 7830–7834.
4 A. Tacca, L. Meda, G. Marra, A. Savoini, S. Caramori, V. Cristino, C. A. Bignozzi, V. G. Pedro, P. P. Boix, S. Gimenez and J. Bisquert, *ChemPhysChem*, 2012, **13**, 3025–3034.
5 Y. Park, K. J. McDonald and K. S. Choi, *Chem. Soc. Rev.*, 2013, **42**, 2321–2337.
6 M. S. Prévot and K. Sivula, *J. Phys. Chem. C*, 2013, **117**, 17879–17893.
7 N. S. Sariciftci, L. Smilowitz, A. J. Heeger and F. Wudl, *Science*, 1992, **258**, 1474–1476.
8 M. A. Green, K. Emery, Y. Hishikawa, W. Warta and E. D. Dunlop, *Prog. Photovoltaics*, 2012, **20**, 12–20.
9 Z. He, C. Zhong, S. Su, M. Xu, H. Wu and Y. Cao, *Nat. Photonics*, 2012, **6**, 591–595.
10 J. Danziger, J. P. Dodelet and N. R. Armstrong, *Chem. Mater.*, 1991, **3**, 812–820.
11 V. Gautam, M. Bag and K. S. Narayan, *J. Phys. Chem. Lett.*, 2010, **1**, 3277–3282.
12 C. Janaky, N. R. de Tacconi, W. Chanmanee and K. Rajeshwar, *J. Phys. Chem. C*, 2012, **116**, 4234–4242.
13 E. Lanzarini, M. R. Antognazza, M. Biso, A. Ansaldo, L. Laudato, P. Bruno, P. Metrangolo, G. Resnati, D. Ricci and G. Lanzani, *J. Phys. Chem. C*, 2012, **116**, 10944–10949.
14 G. Suppes, E. Ballard and S. Holdcroft, *Polym. Chem.*, 2013, **4**, 5345–5350.
15 Z. F. Wang, P. Xiao, L. Qiao, X. Q. Meng, Y. H. Zhang, X. L. Li and F. Yang, *Phys. B*, 2013, **419**, 51–56.
16 T. Yohannes, T. Solomon and O. Inganas, *Synth. Met.*, 1996, **82**, 215–220.
17 W. A. Gazotti, A. F. Nogueira, E. M. Girotto, M. C. Gallazzi and M. A. De Paoli, *Synth. Met.*, 2000, **108**, 151–157.
18 A. Sergawie, T. Yohannes, S. Günes, H. Neugebauer and N. S. Sariciftci, *J. Braz. Chem. Soc.*, 2007, **18**, 1189–1193.
19 P. P. Boix, A. Guerrero, L. F. Marchesi, G. Garcia-Belmonte and J. Bisquert, *Adv. Energy Mater.*, 2011, **1**, 1073–1078.
20 P. P. Boix, G. Garcia-Belmonte, U. Munecas, M. Neophytou, C. Waldauf and R. Pacios, *Appl. Phys. Lett.*, 2009, **95**, 233302.
21 G. F. A. Dibb, M.-A. Muth, T. Kirchartz, S. Engmann, H. Hoppe, G. Gobsch, M. Thelakkat, N. Blouin, S. Tierney, M. Carrasco-Orozco, J. R. Durrant and J. Nelson, *Sci. Rep.*, 2013, **3**, 3335.
22 A. Guerrero, L. F. Marchesi, P. P. Boix, S. Ruiz-Raga, T. Ripolles-Sanchis, G. Garcia-Belmonte and J. Bisquert, *ACS Nano*, 2012, **6**, 3453–3460.
23 F. E. Osterloh, M. A. Holmes, L. L. Chang, A. J. Moule and J. Zhao, *J. Phys. Chem. C*, 2013, **117**, 26905–26913.
24 I. Mora-Sero, L. Bertoluzzi, V. Gonzalez-Pedro, S. Gimenez, F. Fabregat-Santiago, K. W. Kemp, E. H. Sargent and J. Bisquert, *Nat. Commun.*, 2013, **4**, 2272.
25 R. A. Marcus, *J. Chem. Phys.*, 1956, **24**, 966–978.
26 R. A. Marcus, *Rev. Mod. Phys.*, 1993, **65**, 599–610.
27 K. Ziemelis, A. Hussain, D. Bradley, R. Friend, J. Rühe and G. Wegner, *Phys. Rev. Lett.*, 1991, **66**, 2231.
28 R. Österbacka, C. An, X. Jiang and Z. Vardeny, *Science*, 2000, **287**, 839–842.
29 M. Antognazza, D. Ghezzi, D. Musitelli, M. Garbugli and G. Lanzani, *Appl. Phys. Lett.*, 2009, **94**, 243501.
30 K. M. Noone, S. Subramaniyan, Q. Zhang, G. Cao, S. A. Jenekhe and D. S. Ginger, *J. Phys. Chem. C*, 2011, **115**, 24403–24410.
31 K. M. Noone, E. Strein, N. C. Anderson, P.-T. Wu, S. A. Jenekhe and D. S. Ginger, *Nano Lett.*, 2010, **10**, 2635–2639.
32 X. Y. Chin, J. Yin, Z. Wang, M. Caironi and C. Soci, *Sci. Rep.*, 2014, **4**, 3626.
33 E. A. Santori, N. C. Strandwitz, R. L. Grimm, B. S. Brunschwig, H. A. Atwater and N. S. Lewis, *Energy Environ. Sci.*, 2014, **7**, 2329–2338.
34 F. Fabregat-Santiago, G. Garcia-Belmonte, I. Mora-Sero and J. Bisquert, *Phys. Chem. Chem. Phys.*, 2011, **13**, 9083–9118.
35 D. Ghezzi, M. R. Antognazza, R. Maccarone, S. Bellani, E. Lanzarini, N. Martino, M. Mete, G. Pertile, S. Bisti, G. Lanzani and F. Benfenati, *Nat. Photonics*, 2013, **7**, 400–406.

36 T. Ripolles-Sanchis, A. Guerrero and G. Garcia-Belmonte, *Appl. Phys. Lett.*, 2013, **103**, 243306.
37 A. M. Nardes, M. Kemerink, M. M. de Kok, E. Vinken, K. Maturova and R. A. J. Janssen, *Org. Electron.*, 2008, **9**, 727–734.
38 X. Jiang, F. L. Wong, M. K. Fung and S. T. Lee, *Appl. Phys. Lett.*, 2003, **83**, 1875–1877.
39 *Encyclopedia of Electrochemistry, Semiconductor Electrodes and Photoelectrochemistry*, ed., A. J. Bard, M. Stratmann and S. Licht, Wiley-VCH, 2002, vol. 6.
40 J. Ajuria, I. Etxebarria, W. Cambarau, U. Munecas, R. Tena-Zaera, J. C. Jimeno and R. Pacios, *Energy Environ. Sci.*, 2011, **4**, 453–458.
41 P. P. Boix, J. Ajuria, I. Etxebarria, R. Pacios, G. Garcia-Belmonte and J. Bisquert, *J. Phys. Chem. Lett.*, 2011, **2**, 407–411.
42 J. L. Dempsey, B. S. Brunschwig, J. R. Winkler and H. B. Gray, *Acc. Chem. Res.*, 2009, **42**, 1995–2004.
43 X. Hu, B. M. Cossairt, B. S. Brunschwig, N. S. Lewis and J. C. Peters, *Chem. Commun.*, 2005, 4723–4725.
44 C. N. Valdez, J. L. Dempsey, B. S. Brunschwig, J. R. Winkler and H. B. Gray, *Proc. Natl. Acad. Sci. U. S. A.*, 2012, **109**, 15589–15593.
45 A. Fihri, V. Artero, M. Razavet, C. Baffert, W. Leibl and M. Fontecave, *Angew. Chem.*, 2008, **120**, 574–577.
46 M. Razavet, V. Artero and M. Fontecave, *Inorg. Chem.*, 2005, **44**, 4786–4795.